Plasma Science and Technology

PAPER

Analysis of an Ar plasma jet in a dielectric barrier discharge conjugated with a microsecond pulse

Plasma Sci. Technol. **21** (2019) 095401 (9pp) https://doi.org/10.1088/2058-6272/ab1d45

Analysis of an Ar plasma jet in a dielectric barrier discharge conjugated with a microsecond pulse

Duc Ba NGUYEN[1,2], Quang Hung TRINH[2], Won Gyu LEE[3] and Young Sun MOK[1]

[1] Department of Chemical and Biological Engineering, Jeju National University, Jeju 63243, Republic of Korea
[2] Center for Advanced Chemistry, Institute of Research and Development, Duy Tan University, 03 Quang Trung, Da Nang, Vietnam
[3] Division of Chemical Engineering and Bioengineering, Kangwon National University, Chuncheon, Kangwon 24341, Republic of Korea

E-mail: smokie@jejunu.ac.kr

Received 29 December 2018, revised 20 April 2019
Accepted for publication 28 April 2019
Published 28 June 2019

Abstract

In this work, an Ar plasma jet generated by an AC-microsecond-pulse-driven dielectric barrier discharge reactor, which had two ring-shaped electrodes isolated from the ambient atmosphere by transformer oil, was investigated. By special design of the oil insulation, a chemically active Ar plasma jet along with a safe and stable plasma process as well as low emission of CO and NO_x were successfully achieved. The results indicated that applied voltage and frequency were basic factors influencing the jet temperature, discharge power, and jet length, which increased significantly with the two operating parameters. Meanwhile, gas velocity affected the jet temperature in a reverse direction. In comparison with a He plasma jet, the Ar plasma jet had relatively low jet temperature under the same level of the input parameters, being preferable for bio-applications. The Ar plasma jet has been tested to interact with human skin within 5 min without the perception of burnt skin and electrical shock.

Keywords: Ar plasma jet, atmospheric pressure plasma jet, OES of Ar, gas emission of Ar plasma jet, transformer oil

(Some figures may appear in colour only in the online journal)

1. Introduction

Atmospheric pressure plasma jets (APPJs) have been researched heavily for the last two decades because of their great potential for many applications ranging from material processing to medical treatment [1–9]. The commonly used configuration to generate APPJs is the coplanar-coaxial dielectric barrier discharge (DBD) with two ring-shaped electrodes wrapped outside a dielectric tube [10, 11]. Noble gases, such as helium (He), argon (Ar), and neon (Ne), are frequently utilized as the discharge gas [11–13].

One of the unique properties of APPJs is the long plasma active column (i.e. plasma jet) downstream outside of the inter-electrode space, which enables them to be used flexibly to treat objects of different shapes and sizes. A plasma jet is composed of a series of discrete plasma pockets, called plasma bullets, travelling at a speed of several to hundreds km s^{-1}, which is much higher than the gas velocity [14–17]. The emission of high-speed plasma bullets makes plasma jets continuous to the naked eye to the length of several centimeters [17–19]. Generally, the plasma jet length increases with the external electric field strength, and therefore the voltage applied on the electrodes [16]. Increasing the applied voltage is, however, limited by the ignition of spark and subsequently arc in the air gap between the electrodes [20]. Arcing restricts the electrical power delivered to plasma jets and causes safety problems. Replacing the air space between and surrounding the electrodes by an electrical insulator is the only way to solve the

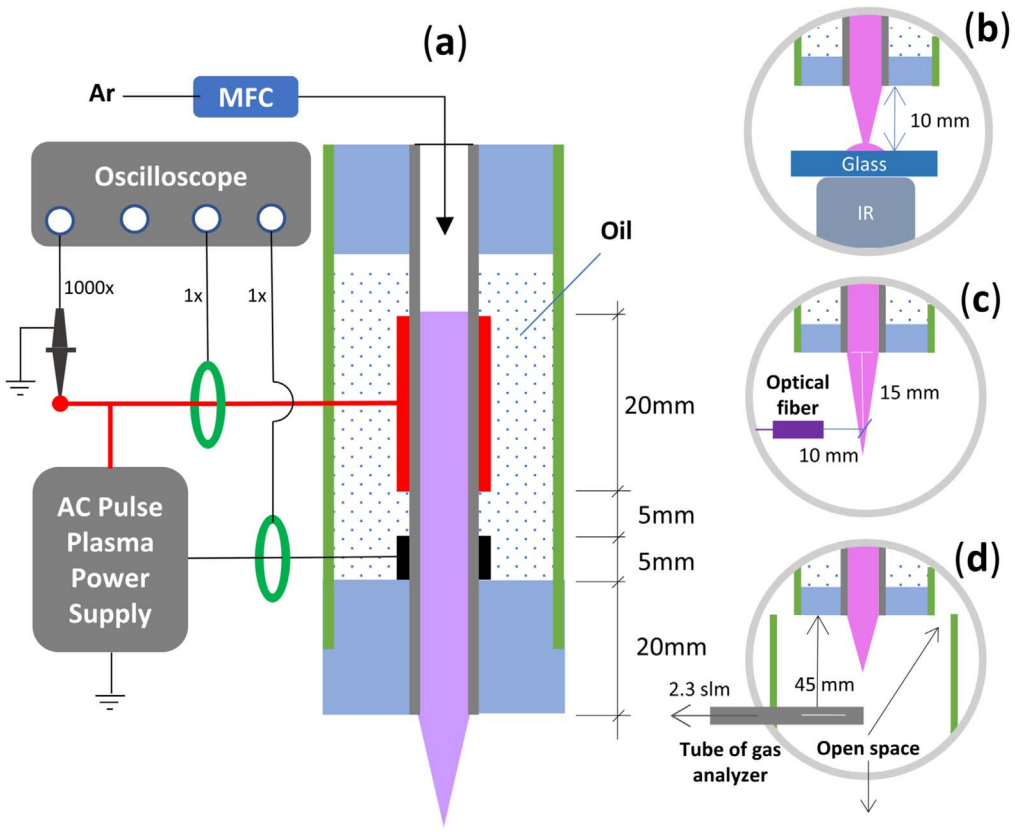

Figure 1. (a) A schematic diagram of the experimental setup for the Ar plasma jet, (b) measurement of the jet temperature, (c) optical emission spectra, and (d) gas emission.

issue. Solid materials, such as glass, ceramics, and Teflon, are widely used as a high-voltage insulator with very high dielectric strength. However, the electrode-surrounding air is usually not eliminated completely by using solid insulators, since there is still a thin air layer existing between an insulator and electrode when they are mechanically assembled. Also, there are always voids and cracks as electrodes are alternatively insulated by the coating methods, for example with ceramics [21]. Liquid electrical insulating materials (e.g. transformer oils) are therefore considered suitable for the insulation purposes of plasma electrodes. Insulating oils not only possess high breakdown voltages but they also have excellent flexibility enabling them to completely cover and isolate the electrodes from the ambient air. Recently, we have been successful in using electrical insulating oils other than solid candidates for insulating the ground electrode of a coaxial rod-to-cylinder type reactor, and achieved a stable, high performance for CO_2 reforming of CH_4 to syngas [22]. By using insulating oils, power loss due to unwanted sparking is minimized and the heat generated from plasma discharge and dielectric heating can be dissipated more easily. This is beneficial to the formation of APPJs, especially for biomedical applications, since the operation safety and gas temperature control could be greatly improved.

In this study, we demonstrated a stable Ar plasma jet generated by a DBD reactor with two ring-type electrodes immersed in transformer oil. The characteristics of the plasma jet in terms of jet length, jet temperature, discharge power, and composition of emission gases were investigated experimentally in response to simultaneous variation of applied voltage and gas flow rate, as well as applied voltage and frequency, to determine the optimum conditions for operation or the input parameters for bio-applications. A comparison between Ar and He plasma jets on the jet length and jet temperature was made by variation of the gas velocity conjugated with the applied voltage.

2. Experimental

Figure 1 shows a schematic diagram of the DBD reactor with two ring-type electrodes for generating an Ar plasma jet. The two electrodes were isolated from the ambient air by electrical insulating oil, which has been described elsewhere [20]. Briefly, the quartz capillary tube had the inner and outer diameters of 2 and 4 mm, respectively. The two ring electrodes were stainless steel tubes; these had inner and outer diameters of 4 and 6 mm, respectively. To generate a plasma jet effectively, a short ground electrode and distance between the electrodes were proposed [20, 23]. Therefore, in this study, the power electrode was made 20 mm long, while it was 5 mm for the length of the ground electrode. The two electrodes were coaxially assembled outside the quartz tube with the distance between them and the distance from the lower end of the ground electrode to the nozzle exit being 5 and 20 mm, respectively. To generate plasma, Ar with a

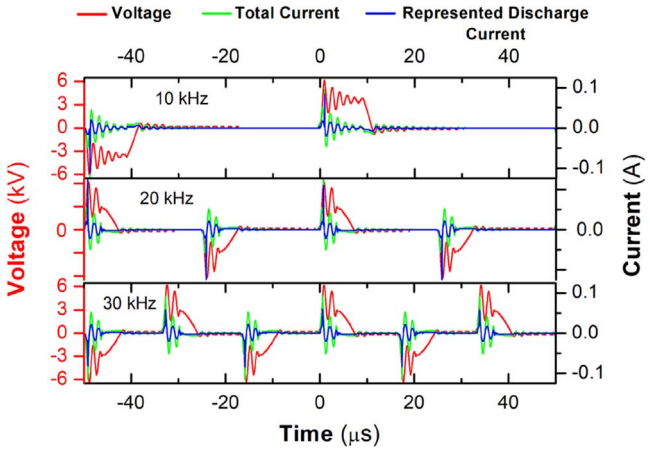

Figure 2. Voltage, total current (high-voltage wire current), and represented discharge current (ground wire current) under various applied frequencies at an applied voltage of 6 kV and total flow rate of 3 slm.

purity of 99.99% was introduced to the reactor by a mass flow controller (AFC 500, AFC Co., Korea), while high voltage on the power electrode was supplied by an AC pulse power supply (HVP, AP Plasma Power Supply, Korea). The plasma power supply can provide voltage up to 15 kV and frequency from 5 to 30 kHz. During the plasma process, various jet parameters and properties were examined, including jet length, jet temperature, optical emission spectra, and emission of NO_x and CO. The jet length was measured from the nozzle exit to the jet tip by a ruler placed parallel to the plasma jet. The jet temperature was measured by an infrared thermometer (IRtech, IR4, Korea) at 10 mm from the nozzle exit (figure 1(b)). To examine the Ar plasma jet, the optical emission spectra and gas emission were analyzed by an optical emission spectrometer (OES, AvaSpec-2048 XL, Netherlands) and by a gas analyzer (Ecom®, MK 6000, Korea), respectively. In detail, the optical fiber tip was located 15 mm from the nozzle exit and 10 mm from the tube axis (figure 1(c)); the probe tip of the gas analyzer was located 45 mm from the nozzle exit, and the total flow rate of the gas pump was 2.3 slm (figure 1(d)).

To determine the discharge power, the applied voltage and current data were recorded by an oscilloscope (Tektronix, TBS1064, four channels, 60 MHz, 1 GS s^{-1}). The oscilloscope was equipped with a passive high-voltage probe (Tektronix, P6015A, USA) to measure applied voltage and a current monitor (Pearson Electronics, 2100, USA) to measure currents (the probe was located at the high-voltage wire for the total current and the ground wire for the represented discharge current). Figure 2 shows typical waveforms of voltage and currents during the plasma process with changing applied frequency. Under various applied frequencies from 10 to 30 kHz and at an applied voltage of 6 kV, the current pulse widths, which correspond to two high-voltage peaks in each voltage phase, were maintained at around 3.35 μs. The typically represented discharge currents were similar to the total currents; however, their intensities were slightly lower than those of the total currents as the total current was the sum of the represented discharge current and upstream/downstream currents. To obtain high accuracy of the discharge power estimation of a DBD plasma jet, the current probe should be located at the discharge zone or high-voltage wire instead of at the grounded wire [24]. Consequently, a discharge power was calculated by integrating the product of the applied voltage and total current (equation (1)).

$$\text{Discharge power, } P_{\text{avg}}(W) = f\int_{-\frac{T}{2}}^{+\frac{T}{2}} v(t)\, i(t)\, \mathrm{d}t \qquad (1)$$

3. Results and discussion

3.1. Effects of input parameters on the plasma jet

Figure 3 shows the evolution of plasma jet output parameters with the changes in the applied voltage and gas flow rate, which indicates that the effect of applied voltage on the Ar plasma jet output parameters, namely jet length, jet temperature, and discharge power, was superior to that of the gas flow rate. Specifically, an increase in the applied voltage from 5 to 8 kV resulted in significant increases in jet length, jet temperatures, and discharge power, whereas these parameters slightly changed with the gas flow rate from 2 to 5 slm (gas velocity: 10.61–26.52 m s^{-1}), except for the jet temperature, which largely decreased with augmentation of the gas flow rate at a high applied voltage. Applied voltage, as well as frequency, is a basic factor in determining the input energy, and therefore the discharge power. The increase in the applied voltage enhances the external electrical field, resulting in a higher density and energy of electrons and more metastable species produced in the discharge zone. These, in turn, promote the speed of plasma bullets as well as plasma jet length [25–27]. During the plasma process, part of the input energy was used to heat the discharge gas and plasma reactor, which led to the increase in the gas temperature in the jet region. Moreover, energy consumption for heating the plasma gas and reactor may be a cause of the non-linear relationship between voltage and the ratio of length to power, as shown in figure 3(d). In this plasma system, the Ar plasma jet length more or less decreased when the gas velocity was above 15.92 m s^{-1} (flow rate: 3 slm). The phenomena are in line with those of a previous study [28]. Specifically, as the gas velocity was raised from 3 to 5 slm at 5 kV (i.e. gas velocity from 15.92 to 26.52 m s^{-1}), Ar plasma jet propagation decreased from 18 to 14 mm in length and the jet appearance changed from a laminar flow to a turbulent form. The increase in gas flow rate along with the reduction in jet temperature resulted in a higher pressure build-up or larger number density of plasma gas, which is considered one of the factors contributing to the decrease in jet length. The optimum gas flow rate for the jet length was found to be 3 slm for the whole range of applied voltages.

Besides the gas flow rate, the effect of power frequency along with applied voltage on the plasma jet was examined and is shown in figure 4. In this experiment, the gas flow rate was kept constant at 3 slm, while the frequency varied from 10 to 30 kHz with intervals of 10 kHz. As can be seen from

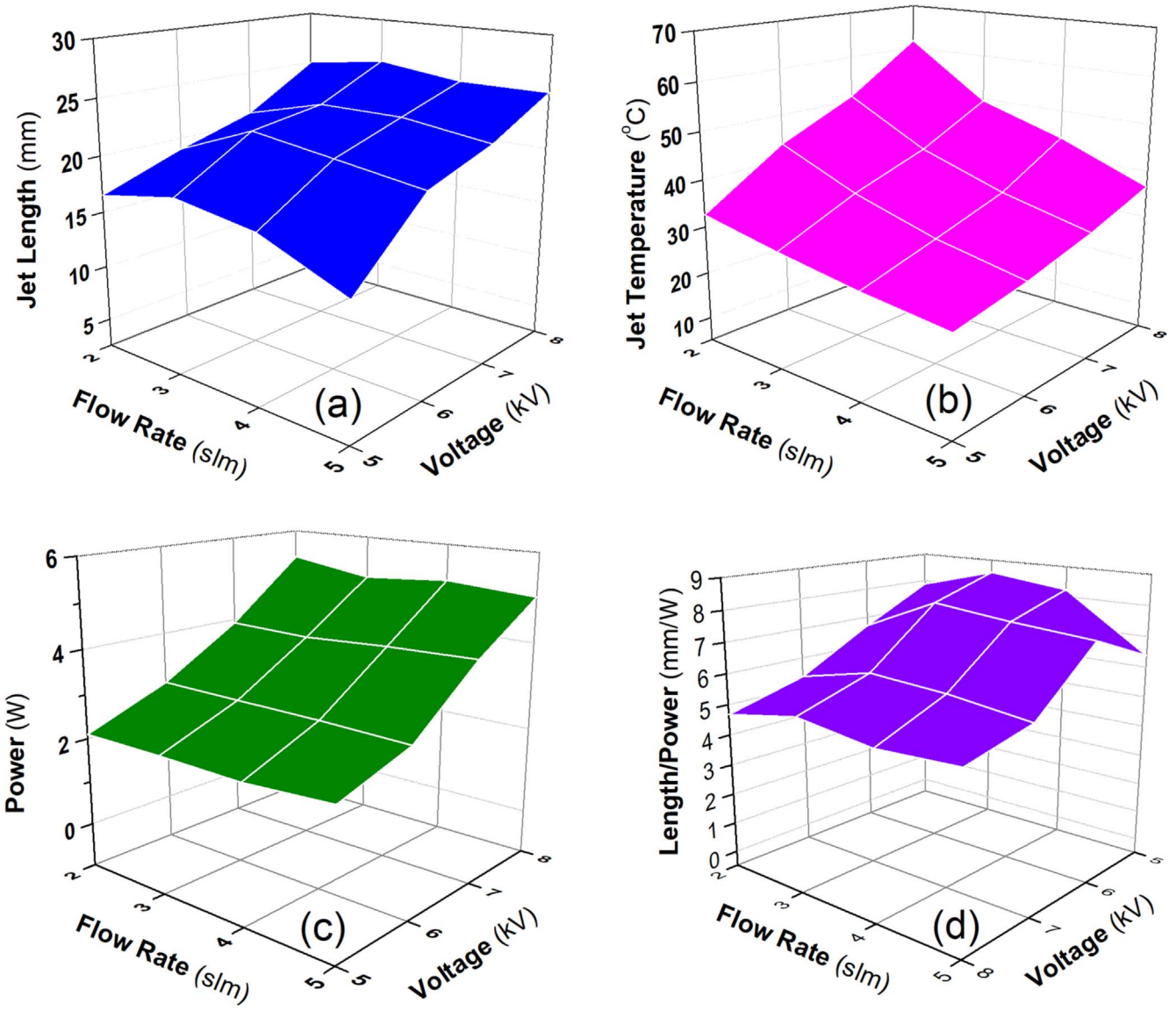

Figure 3. The effect of gas flow rate and applied voltage on (a) jet length, (b) jet temperature, (c) discharge power, and (d) the ratio of jet length to discharge power (frequency: 30 kHz; temperature recorded after 5 min of plasma ignition).

figures 4(a) to (c), similar to the influence of applied voltage, raising the frequency generally increased the jet length, jet temperature, and discharge power. For jet length, the influence of frequency was more noticeable at low applied voltage. For example, at an applied voltage of 6 kV, the jet length was increased from 18 to 22 mm as the frequency increased from 10 to 30 kHz. Meanwhile, at a higher applied voltage of 8 kV, the jet length slightly changed from 25 to 26 mm. The same was true for the effect of applied voltage at various gas velocities. The jet temperature and discharge power significantly increased as the applied voltage and frequency were both raised. The change in jet length could be explained in terms of seed electron density. The plasma bullet propagation and therefore plasma jet length are strongly dependent on the temporal and spatial distribution of seed electron density, which rapidly decays during a time period between two consecutive current pulses and along the jet axis [29]. At low frequency and applied voltage, the seed electron density should be low, which corresponds to a short jet length. Raising either the frequency or applied voltage results in shortening of the period between two consecutive pulses or increasing the initial seed electron density, which, in turn, increases the seed electron density just before the following pulse or bullet. At high frequency and applied voltage, the effect of changing these parameters should be less since the seed electron density approaches its saturated value. As a result of variation in the jet length and discharge power, the desire for increasing the specific jet length or the ratio of jet length to discharge power is effective with the frequency variation (see figure 4(d)).

3.2. Evaluation of the plasma jet carried out by the reactor

Figure 5 demonstrated that the Ar plasma jet generated by the reactor used in this work was a chemically active source potentially used for many applications. This comes from the

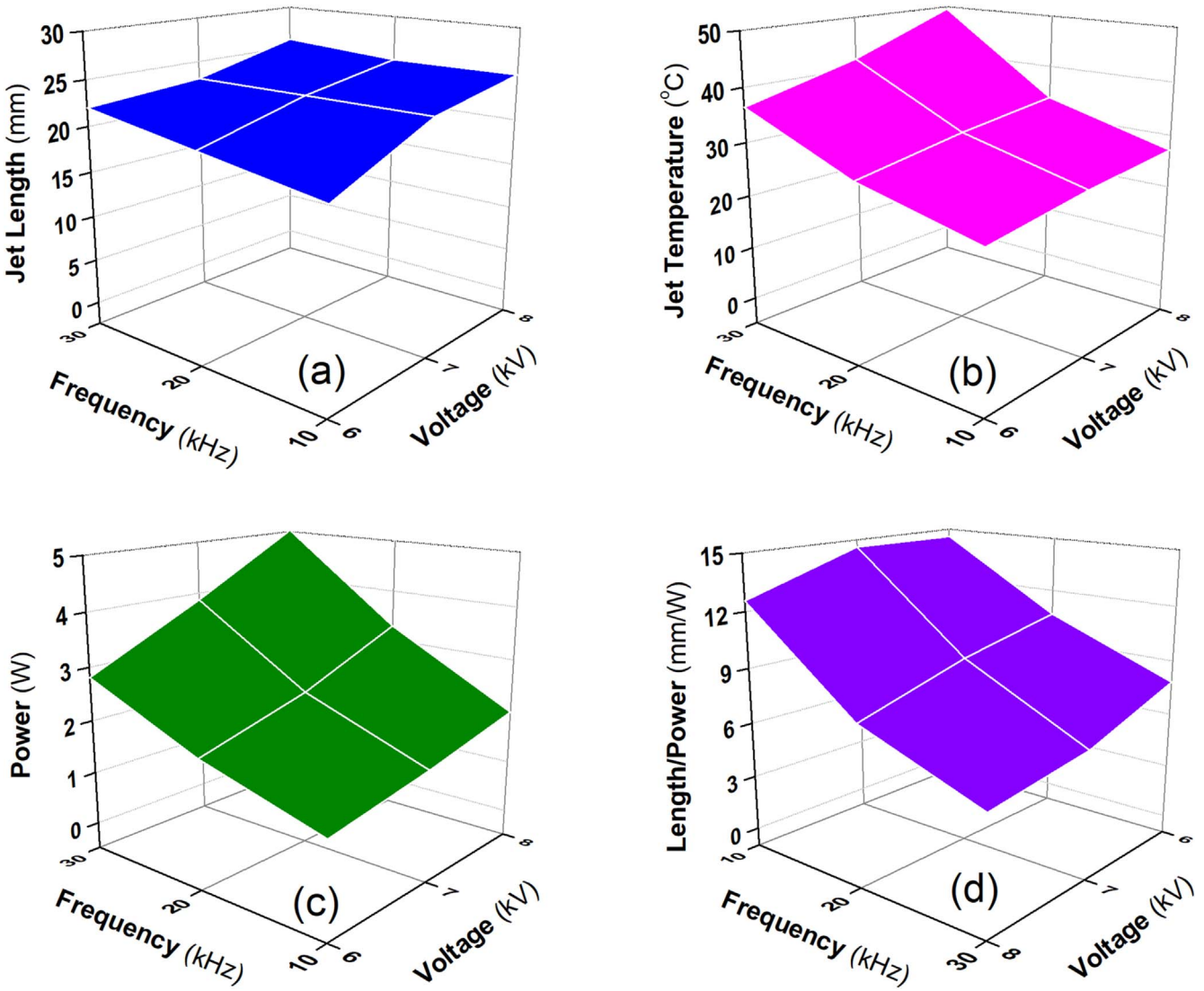

Figure 4. The effect of frequency and applied voltage on (a) jet length, (b) jet temperature, (c) discharge power, and (d) the ratio of jet length to discharge power (flow rate: 3 slm; temperature recorded after 5 min of plasma ignition).

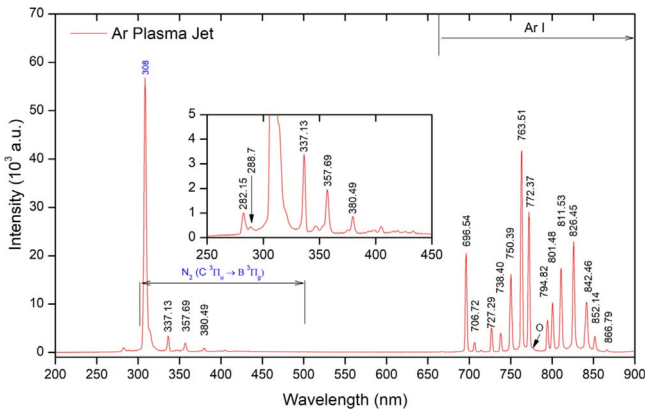

Figure 5. Optical emission spectra of the Ar plasma jet (applied voltage: 7 kV; frequency: 30 kHz; Ar flow rate: 2 slm; Ar purity: 99.999%).

spectrum of the Ar plasma jet, which consisted of several intense peaks of excited active species, including Ar, N_2, N_2^+, O, and OH. Indeed, the Ar lines with high intensities emitted by the plasma jet were observed in the wavelength range from 690 to 900 nm. The interaction between the Ar plasma jet and the ambient air resulted in strong lines of N_2 in the second positive system ($C^3\Pi_u \rightarrow B^3\Pi_g$). In addition, several other species, such as N_2^+ in the first negative system ($B\ ^2\Sigma_u^+ \rightarrow X\ ^2\Sigma_g^+$), OH with the most intense peak overlapping with N_2 at 308 nm, and atomic oxygen at 777 nm, were also detected. In this spectrum, NO lines were not clearly identified in the range of 200–300 nm ($A^2\Sigma^+ \rightarrow X^2\Pi$). The results are in line with several Ar plasma jet spectra in previous reports [12, 26, 30, 31]. In comparison with the He plasma jet spectrum carried out by the same system [20], the line intensities of N_2 and N_2^+ of the Ar plasma jet were lower than those of the He plasma jet. Here, we propose one of the reasons is that the excitation energy of He is higher than that of Ar. The formation of excited N_2 and N_2^+ (i.e. reactive nitrogen species, RNS) in Ar and He plasmas results from the collisions of N_2 with electrons and/or metastable species. The average electron energy generated by DBD systems is in the order of a few eV [32]. Meanwhile, it can be seen from the

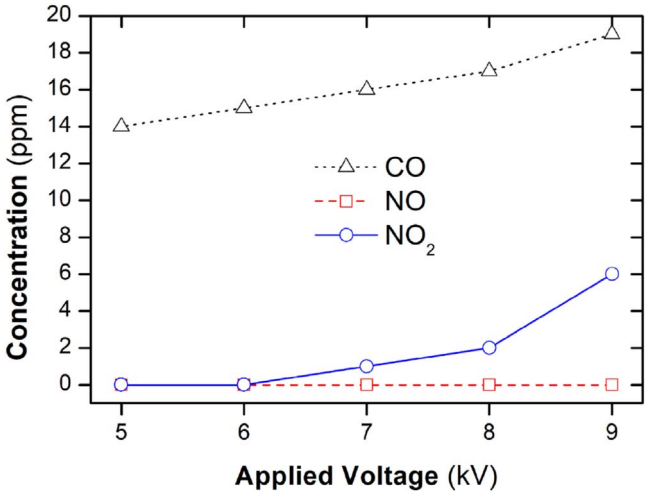

Figure 6. Emission of CO and NO_x during the plasma process under varying applied voltage (applied frequency: 30 kHz; Ar flow rate: 2 slm; the flow rate of the gas pump of the gas analysis: 2.3 slm; Ar purity: 99.99%).

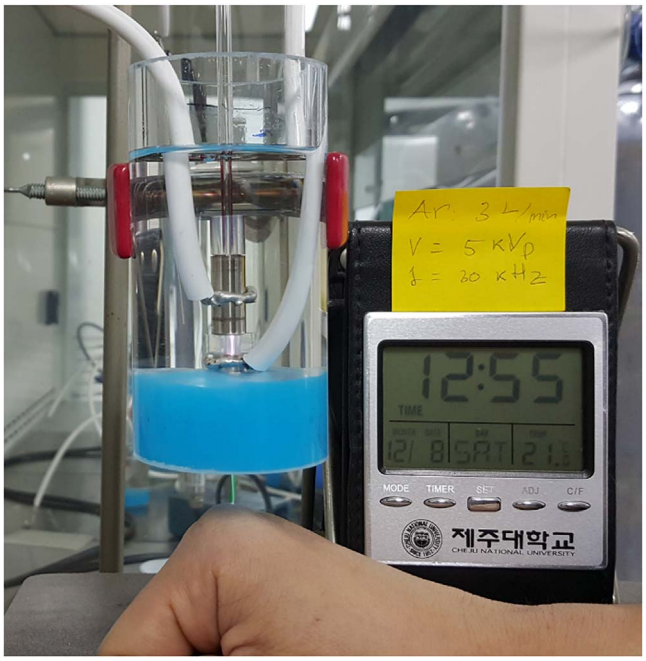

Figure 7. The Ar plasma jet interaction with human skin (applied voltage: 5 kV; frequency: 30 kHz; Ar flow rate: 3 slm).

OES analyses that the spectrum of He plasma locates in the shorter wavelength region (higher energy level) than that of Ar plasma, indicating that the He species have higher energy than the Ar species. That is why the intensities of N_2 and N_2^+ with the Ar plasma are weaker than those with the He plasma. The metastable energies of He and Ar are reported to be around 20 eV and 11.6 eV, respectively [33]. Consequently, the significant difference in the line intensities of N_2 and N_2^+ between the two plasmas is mainly attributed to the higher metastable energy of He than that of Ar. This phenomenon was also found in analyses of CHF_3/O_2 plasma generated by a concentric rod-to-cylinder type of DBD reactor with either Ar, N_2, or He as the dilution gas, wherein He dilution was more accessible to analyze the optical emission spectra [34]. To sum up, the Ar plasma jet generated by the reactor system presented in this work can be considered as a source for low-temperature plasma, which consists of several chemically active species, such as excited Ar and N_2, N_2^+, O, and OH radicals.

To be useful for bio-applications such as human skin treatment, a plasma source must not only have low jet temperature and good electrical safety but also low emissions of hazardous chemicals, e.g. NO_x (NO and NO_2) and CO. In this study, the emission of NO_x and CO by the plasma jet interacting with the ambient air was examined by varying the applied voltage from 5 to 9 kV. The concentrations of emitted NO_x and CO during the plasma process are shown in figure 6. This figure demonstrates that the contents of plasma-induced NO_x and CO were lower than 20 ppm. Specifically, NO was not detected under the experimental conditions in this work. When the applied voltage was smaller than or equal to 6 kV, NO_2 was also under the detection limit of the measuring equipment; however, its concentration rose from 1 to 6 ppm as the applied voltage increased from 7 to 9 kV. The results are similar to those observed with the He plasma jet generated using the same system [20]. A preliminary test of the plasma jet interacting with human skin was also performed and is shown in figure 7. There was no perception of burnt skin and electrical shock in 5 min of interaction; therefore, the plasma source is promising for bio-applications.

3.3. Comparison of Ar and He plasma jets

A comparison of Ar and He plasma jets regarding jet length and temperature varying with gas flow rate at the applied voltages of 5 and 6 kV is shown in figure 8. For the Ar plasma jet, the higher the applied voltage, the longer the jet length, as also seen from figure 3(a). A similar result was observed for the He plasma jet with the gas flow rate in the range of 2–3 slm. However, at a flow rate of 4 slm, the He jet length did not depend on the applied voltage, as the jet length approached similar values for both applied voltages. In contrast to He, Ar has a much larger Townsend's first ionization coefficient, which rises more steeply with an electric field and therefore applied voltage. As a result, raising the applied voltage generally produces more intense filamentary Ar discharge [20, 31, 34]. In addition, compared to the He plasma jet, the Ar plasma jet generally had a shorter length under the same working conditions, except at low values of gas flow rate of 2–3 slm and applied voltage of 5 kV, under which the jet lengths seemed to be identical. Also, in the investigated range, the He plasma jet exhibited a continuous increase in jet length with the gas flow rate. Meanwhile, Ar plasma, as aforementioned, saturated after 3 slm, regardless of applied voltage. Similar to those of traditional coplanar-coaxial DBD plasma jets, the jet length of the plasma system in this work was dependent on the status of the gas flow (i.e. laminar or turbulent mode). In the laminar mode, the jet length increases with the gas flow rate, while it becomes shorter in the turbulent mode [16, 28, 35]. The flow status can be evaluated

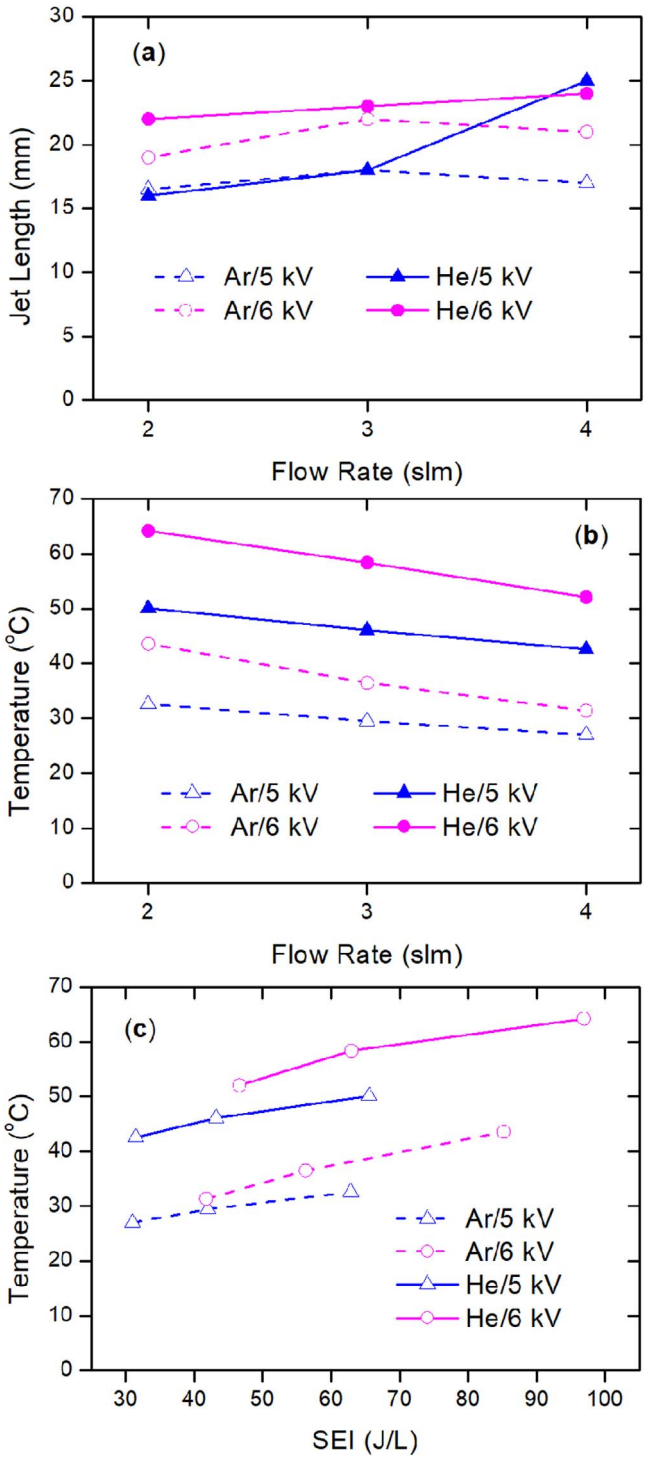

Figure 8. A comparison between Ar and He plasma jets under various flow rates conjugated with applied voltage (applied frequency: 30 kHz; total flow rate: 2–4 slm; the consumed power at 5 and 6 kV approached 2 and 3 W, respectively).

using the formula of the Reynolds number, *Re* [36]:

$$Re = \frac{\rho Q D}{A\mu} \tag{2}$$

where ρ is the gas density (Ar: $1.6228\,\mathrm{kg\,m^{-3}}$, He: $0.1625\,\mathrm{kg\,m^{-3}}$ [37]), Q is the gas flow rate in $\mathrm{m^3/s}$, D is the inner diameter of the quartz capillary tube (2×10^{-3} m), A is the cross-sectional area of the tube ($3.14 \times 10^{-6}\,\mathrm{m^2}$), and μ is the dynamic viscosity (Ar: $2.125 \times 10^{-5}\,\mathrm{kg/m \cdot s}$, He: $1.99 \times 10^{-5}\,\mathrm{kg/m \cdot s}$ [37]). With the dimensions of the tube shown above and the critical value of *Re* for a change from laminar flow to turbulent flow being 2320 [38], the critical gas flow rates for Ar and He were calculated to be 2.86 and 26.76 slm, respectively. It can be seen that the calculated critical Ar flow rate is close to the optimal value of 3 slm observed in this work; whereas the calculated critical flow rate

of He is much larger than the investigated He flow rate, which explains the continuous increase in the He jet length with the gas flow rate from 2 to 4 slm.

The jet temperature of He was higher than that of Ar under varying total flow rate from 2 to 4 slm with an applied voltage of 5 or 6 kV, as shown in figure 8(b). Herein, the discharge power of the Ar plasma jet was comparable to that of the He plasma jet; interestingly, the temperature of the He plasma jet was superior to the Ar plasma jet. A possible explanation for this might be the relatively high thermal conductivity of He (156.7 mW/m · K at 300 K), which approaches nine times that of Ar (17.9 mW/m · K at 300 K) [39]. Indeed, the change in the temperature of the gas fluid can be estimated by $\Delta T = \frac{E}{nC_p}$, in which E (J) energy delivered to the gas fluid and C_p (J mol^{-1}· K) is the molar heat capacity. Since the thermal conductivity of He is larger than that of Ar, the energy delivered to the He flow would be higher than that of Ar in the same conditions. Meanwhile, their molar heat capacities at constant pressure are similar to each other ($C_p = 20.8$ J mol^{-1} · K at 298.15 K) [40]. Therefore, the temperature increase in He fluid was larger than that in Ar fluid in the same conditions. As a result, at the same level of input energy (specific energy input, SEI), the temperature of He fluid is higher than that of Ar, as shown in figure 8(c). In other words, more input energy has been distributed to the surrounding ambient air by the He fluid. To sum up, the Ar plasma jet can be obtained with a low jet temperature, but He plasma is more stable, since a large portion of the input energy can be distributed to the ambient air.

4. Conclusions

In summary, a stable, chemically active Ar plasma jet promising for bio-applications with low jet temperature, low hazardous chemical emission, and safe usage was successfully generated in this work. The jet length, jet temperature and discharge power generally increased continuously along with the applied voltage and frequency, but not with the gas flow rate. Among these output parameters, the jet temperature was the most sensitive with the change in gas flow rate as it rapidly decreased with increasing the gas flow rate, especially at high applied voltage. Meanwhile, the discharge power seemed to hardly change with the gas flow. The optimum value of the gas flow rate for the jet length was found to be 3 slm. Under the applied voltage of 5 kV, frequency of 30 kHz, and gas flow rate of 3 slm, the plasma jet produced was 18 mm long and reached a temperature of 29.5 °C, thus being suitable for bio-applications, such as human skin treatment.

Acknowledgments

This work was supported by the 2019 Scientific Promotion Program funded by Jeju National University and the R&D Program 'Plasma Advanced Technology for Agriculture & Food (Plasma Farming)' through the National Fusion Research Institute (NFRI), Daejeon, Korea. The authors, D B Nguyen and Q H Trinh, acknowledged financial support from Duy Tan University.

ORCID iDs

Duc Ba NGUYEN https://orcid.org/0000-0002-5018-6531

References

[1] Penkov O V *et al* 2015 *J. Coat. Technol. Res.* **12** 225
[2] Gay-Mimbrera J *et al* 2016 *Adv. Ther.* **33** 894
[3] Mariotti D *et al* 2012 *Plasma Process. Polym.* **9** 1074
[4] von Woedtke T *et al* 2013 *Phys. Rep.* **530** 291
[5] Wu S, Cao Y and Lu X 2016 *IEEE Trans. Plasma Sci.* **44** 134
[6] Michael K 2015 *Plasma Sources Sci. Technol.* **24** 033001
[7] Bruggeman P J *et al* 2016 *Plasma Sources Sci. Technol.* **25** 053002
[8] Deng G L *et al* 2018 *Plasma Sci. Technol.* **20** 115503
[9] Zhang R B *et al* 2017 *Plasma Sci. Technol.* **19** 105505
[10] Brandenburg R 2017 *Plasma Sources Sci. Technol.* **26** 053001
[11] Lu X, Laroussi M and Puech V 2012 *Plasma Sources Sci. Technol.* **21** 034005
[12] Reuter S, von Woedtke T and Weltmann K D 2018 *J. Phys. D: Appl. Phys.* **51** 233001
[13] Yang L L *et al* 2016 *Plasma Sci. Technol.* **18** 912
[14] Ohyama R, Sakamoto M and Nagai A 2009 *J. Phys. D: Appl. Phys.* **42** 105203
[15] Teschke M *et al* 2005 *IEEE Trans. Plasma Sci.* **33** 310
[16] Mericam-Bourdet N *et al* 2009 *J. Phys. D: Appl. Phys.* **42** 055207
[17] Oh J S, Walsh J L and Bradley J W 2012 *Plasma Sources Sci. Technol.* **21** 034020
[18] Liu L J *et al* 2014 *Appl. Phys. Lett.* **104** 244108
[19] Algwari Q T and O'Connell D 2011 *Appl. Phys. Lett.* **99** 121501
[20] Ba Nguyen D, Mok Y S and Lee W G 2019 *IEEE Trans. Plasma Sci.* (https://doi.org/10.1109/TPS.2019.2896666)
[21] Niittymäki M *et al* 2015 DC dielectric breakdown behavior of thermally sprayed ceramic coatings *Proc. 24th Nordic Insulation Symp. on Materials, Components and Diagnostics (Copenhagen, Denmark, 2015)*
[22] Ba Nguyen D and Lee W G 2014 *J. Ind. Eng. Chem.* **20** 972
[23] Zhu P *et al* 2018 *J. Phys. D: Appl. Phys.* **51** 405202
[24] Ba Nguyen D *et al* 2019 *IEEE Trans. Plasma Sci.* (https://doi.org/10.1109/TPS.2019.2894019)
[25] Begum A, Laroussi M and Pervez M R 2013 *AIP Adv.* **3** 062117
[26] Park H S *et al* 2010 *Phys. Plasmas* **17** 033502
[27] Lu X P and Ostrikov K 2018 *Appl. Phys. Rev.* **5** 031102
[28] Li Q *et al* 2009 *Appl. Phys. Lett.* **95** 141502
[29] Wu S, Lu X and Pan Y 2013 *Curr. Appl. Phys.* **13** S1
[30] Lai K L *et al* 2015 *AIP Conf. Proc.* **1657** 150002
[31] Lau Y *et al* 2014 *J. Sci. Technol. Trop.* **10** 131
[32] Zhou L M *et al* 1998 *Energy Fuels* **12** 1191
[33] Wang R X *et al* 2016 *Appl. Surf. Sci.* **367** 401
[34] Nguyen D B and Lee W G 2016 *RSC Adv.* **6** 26505
[35] Yambe K, Furuichi T and Ogura K 2014 Influence of gas flow on plasma length in atmospheric pressure plasma jet *JPS Conf. Proc.* **1** 015084
[36] Lide D R 2010 *CRC Handbook of Chemistry and Physics* 90th edn (Boca Raton, FL: CRC Press)
[37] Selvam M and Thiru S 2014 *J. Eng. Technol.* **5** 105

[38] Shao X J *et al* 2011 *IEEE Trans. Plasma Sci.* **39** 2340
[39] Huber M L and Harvey A H 2010 Thermal conductivity of gases ed D R Lide *CRC Handbook of Chemistry and Physics* 90th edn (Boca Raton, FL: CRC Press)
[40] Lide D R 2010 Standard thermodynamic properties of chemical substances ed D R Lide *CRC Handbook of Chemistry and Physics* 90th edn (Boca Raton, FL: CRC Press)